

Gold Hollow Nanospheres: Tunable Surface Plasmon Resonance Controlled by Interior-Cavity Sizes

Han-Pu Liang,^{†,‡} Li-Jun Wan,^{*,†} Chun-Li Bai,[†] and Li Jiang[§]

Institute of Chemistry, Chinese Academy of Sciences, Beijing 100080, China, and Schlumberger Doll Research, 36 Old Quarry Road, Ridgefield, Connecticut 06877

Received: November 2, 2004; In Final Form: March 1, 2005

Uniform gold hollow nanospheres with tunable interior-cavity sizes were fabricated by using Co nanoparticles as sacrificial templates and varying the stoichiometric ratio of starting material HAuCl_4 over the reductants. The formation of these hollow nanostructures is attributed to two subsequent reduction reactions: the initial reduction of HAuCl_4 by Co nanoparticles, followed by the reduction by NaBH_4 . In addition, a thick layer of silica was successfully coated onto the gold hollow nanospheres. These nanostructures are extensively characterized by TEM, XRD, HRTEM, SEM, electron diffraction, energy-dispersive X-ray analysis, and UV–visible absorption spectroscopy. It is evident that the SPR peak locations corresponding to these hollow nanospheres are shifted over a region of more than 100 nm wavelength due to changes of shell thickness, which make these optically active nanostructures of great interest in both fundamental research and practical applications.

Introduction

Gold nanostructures have attracted considerable interest due to their intriguing surface plasmon resonance (SPR) property originating from the collective oscillation of their conduction electrons in response to optical excitation.¹ These optically active nanostructures are potentially useful in photocrystals, plasmonic waveguides, chemical or biological sensors, optical filters, and optically triggered drug delivery.² Consequently, various gold nanostructures such as nanoparticles, nanowires, hollow nanospheres, and nanoshells were fabricated leading to different and highly sensitive SPR features. In particular, gold hollow nanospheres are intriguing to synthesize and investigate because of their fascinating SPR properties. For example, Xia et al. reported that the SPR spectra of gold hollow spheres exhibit a much more sensitive response toward environmental changes than solid colloids.³ Halas and co-workers have prepared nanoparticles with multiply, concentric shells of gold and silica and gold shell can be used to enable fast whole-blood immunoassays.⁴ As such the SPR frequency is strongly dependent on the size, shape, and surface functionality of the metallic nanostructures. For hollow metallic nanospheres, the frequency is a sensitive function of the inner and outer diameter of the metallic nanospheres.⁵ Therefore, it is necessary to explore metallic hollow nanospheres with tunable cavity size so to affect the SPR property. To date, hollow spheres of various materials have been extensively investigated in the literature,^{6–11} invariably focused on two geometrical parameters: shell thickness and cavity size. Most methods are based on the outward growth of the nanosphere shell. Few were dedicated to the fabrication techniques of hollow nanospheres with tunable cavity size, which may be very useful in the practical application and in the study of basic physics.¹² Recently, we developed a facile

method for one-step, large-scale synthesis of Pt hollow nanospheres with Co nanoparticles as sacrificial templates.¹³ Herein, we extend this approach to fabricate gold hollow nanospheres with tunable cavity size by varying the stoichiometric ratio of HAuCl_4 over the reductant(s). The SPR features of these nanospheres are investigated, showing that SPR peak frequency can be continuously tuned over 100 nm wavelength by controlling the interior-cavity size. Silica-coated gold hollow nanospheres were also fabricated and studied.

Experimental Section

Fabrication of Gold Hollow Nanospheres with Tunable Cavity Size. For the synthesis of gold hollow nanospheres with tunable interior cavity, the Co nanoparticles were first fabricated. The preparation is carried out with the method reported by Kobayashi et al.¹⁴ Briefly, 0.2 mL of 0.4 M CoCl_2 solution was added into 200 mL of deaerated aqueous solution containing 8 mM NaBH_4 and 0.8 mM citric acid to fabricate Co nanoparticles. To avoid the oxidation of the Co nanoparticles in the existence of atmospheric oxygen, high-purity nitrogen was bubbled through the solution during the whole procedure. H_2 was evolved during the reaction and continued for several minutes. When the gas evolution ceased, three as-synthesized Co nanoparticle colloidal solutions with equal volume (30 mL) were transferred to three stirred aqueous solutions, samples A, B, and C with different volumes of 1 mM HAuCl_4 (5, 8, and 18 mL). Prior to these, two solutions with equal volume (30 mL) were sampled in the course of H_2 evolution and also transferred to two stirred aqueous solutions, samples D and E with 12 and 40 mL of 1 mM HAuCl_4 , respectively. The obtained suspension solutions were centrifuged and the precipitates were samples A to E.

Fabrication of Silica-Coated Gold Hollow Nanocomposites. Coating of hollow gold nanospheres with amorphous silica was achieved by using the Stöber method.¹⁵ Briefly, approximately 0.5 mg of the as-synthesized gold hollow nanospheres (sample B) was dispersed into a mixture of 20 mL of

* To whom correspondence should be addressed. Phone and Fax: +86–10–62558934. E-mail: wanlijun@iccas.ac.cn.

[†] Chinese Academy of Sciences.

[‡] Also in the Graduate school of CAS, Beijing, China.

[§] Schlumberger Doll Research.

2-propanol and 3 mL of Millipore water. Under continuous stirring, 0.4 mL of 25% ammonia and 0.036 M tetraethyl orthosilicate (TEOS) were added into this system. After the reaction had proceeded for 2 h, the solution was centrifuged to isolate the precipitate, which was then redispersed into Millipore water.

Characterization Methods. For TEM and SEM measurements, the obtained suspension solutions were centrifuged and the precipitates were collected, washed, dispersed by ultrasonic treatment, and dropped on carbon-coated copper grids. TEM measurement, electron diffraction, and energy-dispersive X-ray analysis (EDAX) were performed with a JEM 2010 transmission electron microscope equipped with energy-dispersive X-ray analyzer (Phoenix). High-resolution TEM images were recorded on a Philips TECNAI F30 operating at 300 kV. Powder X-ray diffraction (XRD) was carried out with a Rigaku D/max-2500, using filtered Cu K α radiation. SEM was carried out with a Hitachi S-4300F field emission scanning electron microscope. UV–visible absorption data were recorded on a UV–vis spectrophotometer (UV-1601 PC, SHIMADZU).

Results and Discussion

Gold Hollow Nanospheres with a Tunable Interior Cavity.

The standard reduction potentials of the AuCl $_4^-$ /Au and Co $^{2+}$ /Co redox couple are 0.994 and -0.277 V vs SHE. In the present study, the reduction potentials of these two redox couples can be obtained according to the Nernst equation. Since the reduction potential of the AuCl $_4^-$ /Au redox couple (0.935 V vs SHE) is much higher than that of the Co $^{2+}$ /Co redox couple (-0.377 V vs SHE), AuCl $_4^-$ will be reduced to Au atoms as soon as Co nanoparticles were added into the solution due to the big gap between the potential of these two redox couples. In addition, because the reduced gold atoms are largely confined to the vicinity of sacrificial template outer surface, the diameter of Co nanoparticles determines that of the resulting gold hollow nanostructures. Therefore, the fabrication of Co nanoparticles is a critical foundation in the whole preparation procedure. In the present study, excess reducing agent (NaBH $_4$) was used to modify the nucleation and growth process, hence optimize the diameter and size distribution of Co nanoparticles as suggested by an early report.¹⁶ After the formation of Co nanoparticles, which is easily observed by the solution color change from transparent to dark, this solution was kept for several minutes to allow excessive NaBH $_4$ to react with water completely.^{13,17} Gold hollow nanostructures were successfully fabricated by subsequently adding Co colloidal solution into aqueous HAuCl $_4$ solutions.

Figure 1a shows a typical TEM image of sample B, where there is strong contrast difference in all of the spheres with a bright center surrounded by a much darker edge, confirming their hollow architecture. The average outer diameter of the hollow nanospheres is statistically measured to be 58.6 ± 4.5 nm by sampling 200 hollow nanospheres. No size separation process was necessary on these hollow nanospheres, as the synthetic protocol already achieved high monodispersity. The inset in Figure 1a is an electron diffraction pattern, in which the concentric rings could be assigned as diffraction from {111}, {200}, {220}, and {311} planes of face-center-cubic (fcc) gold from the centermost ring, respectively. Figure 1b is a typical SEM image of sample B, showing the production of large-scale uniform spherical materials. Figure 2 shows the powder X-ray diffraction Pattern of sample B, and all diffraction peaks could be indexed to an fcc phase of gold according to the JCPDS No. 65-2870.

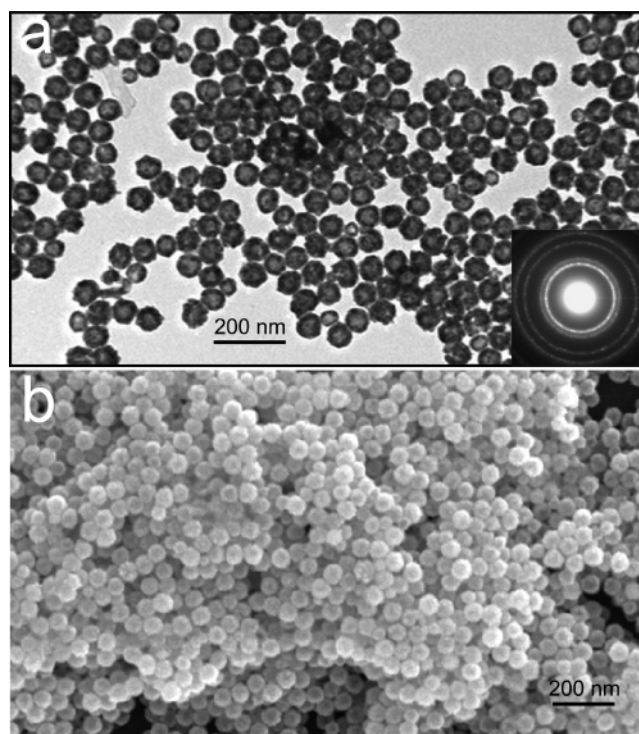


Figure 1. (a) TEM and (b) SEM images of gold hollow nanospheres of sample B. The inset in part a is the electron diffraction pattern obtained on a random assembly of gold nanospheres.

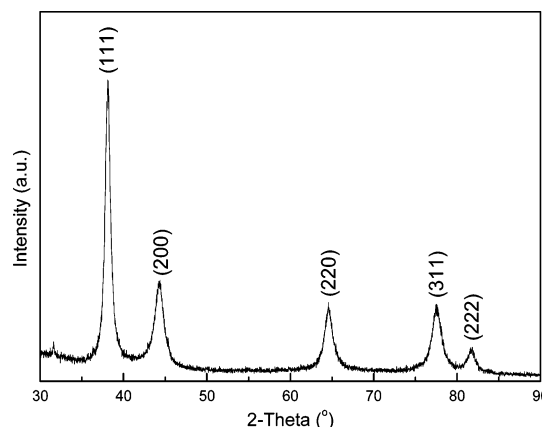
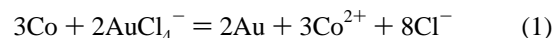


Figure 2. XRD pattern of gold hollow nanospheres (sample B) formed by reducing AuCl $_4^-$ with Co nanoparticles as the sacrifice templates.

Figure 3 is a high-resolution TEM image taken from the surface of an individual gold hollow nanosphere (sample B), from which it is evident that the shell surface of the hollow nanospheres consists of small single Au crystals.

Samples A–C with different volumes of HAuCl $_4$ solutions were designed on the basis of the stoichiometric relationship as presented in eq 1.



The amount of HAuCl $_4$ in sample B is just sufficient to react with the added Co nanoparticles completely, while the ratio of HAuCl $_4$ in sample A and sample C is lower and higher than that in sample B, respectively. Parts a and b of Figure 4 show low-magnification TEM images of samples A and C. Compared with Figure 1a of sample B, obvious changes occur in the shell thickness of these hollow nanospheres. The formation of sample A in Figure 4a with different shell thickness may be attributed

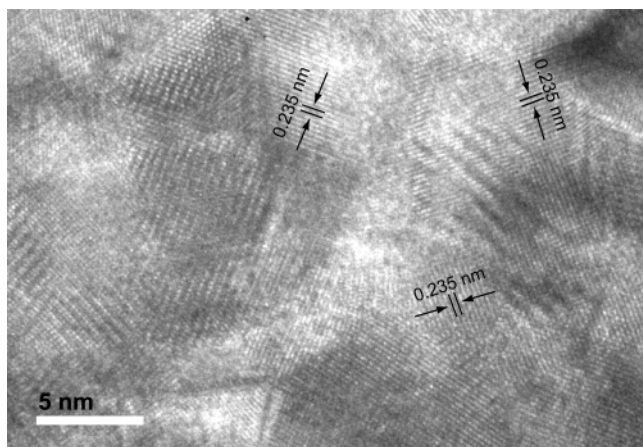


Figure 3. High-resolution TEM images taken from the surface of an individual gold hollow nanosphere (sample B).

to the fact that some Co nanoparticles react with sufficient HAuCl_4 to form a thick shell, while other particles cannot due to the insufficient supply of HAuCl_4 , thus forming a thin shell. As this replacement reaction occurs rapidly, the reduced Au atoms nucleate and grow into very small particles, and eventually evolve into a thin shell around the cobalt nanoparticles. The shells presumably have an incomplete porous structure at an early stage when Co^{2+} and AuCl_4^- are able to continuously diffuse across the shell in reverse directions.¹³ At this stage, the remaining active Co “core” can also be continually oxidized by H^+ , from HAuCl_4 aqueous solution, across the porous shell since the standard reduction potential of the H^+/H_2 redox couple is higher than that of the Co^{2+}/Co redox couple. Compared to eq 1, this reaction is secondary due to the smaller thermodynamic driving force. It is the combination of the two reactions that results in the gold hollow nanostructure without the presence of a Co “core”. From the low-magnification TEM image of sample C in Figure 4b, the gold hollow nanospheres are similar to that of sample B except for additional gold nanoparticles. The high-magnification TEM image in Figure 4c indicates that these nanoparticles are directly connected to the outer shell of

gold hollow spheres. Figure 5 is a proposed mechanism for this formation processes from the observed results. The formation of these nanoparticles may be attributed to the existence of citrate as HAuCl_4 may be reduced by citrate in boiling solution.¹⁸ In the present study, the fact that HAuCl_4 can be reduced by citrate at room temperature may be attributed to the presence of the hollow nanospheres, functioning as “seeds”. These seeds can act as nucleation centers accelerating seed-mediated autocatalytic growth at their surfaces. The reduction reaction is a relatively slow process compared with the replacement reaction. After Co nanoparticles were completely consumed, the porous shell turned into a dense surface as indicated in Figure 3. The change on the shell outer surface may be attributed to the effective reconstruction of Au to form a smooth and highly crystalline structure through the Ostwald ripening process to lower surface energy after Co nanoparticles were completely consumed.^{11b} The dense shell structure no longer allows citrate molecules to diffuse freely across the shell into the cavity, resulting in excess HAuCl_4 reduction on the outer surfaces of the shells and hence the different morphology of sample C. The above mechanism is corroborated by a control experiment, in which an aqueous suspension of sample B was added into HAuCl_4 , resulting in identical composition of obtained solution to that of sample C. The TEM image (not shown) revealed that the morphology of the obtained nanostructures was indeed closely analogous to that of sample C.

Parts d, e, and f of Figure 4 show HMTEM images of samples B, D, and E. Samples D and E, with a higher stoichiometric ratio of HAuCl_4 than that of sample B, were designed to investigate the influence of excess NaBH_4 . From these images gold hollow nanospheres with different shell thickness and interior cavity are evident. Note that the outer surfaces of these hollow spheres are smooth and different from those of sample C. As shown in Figure 4d, these nanospheres clearly exhibit hollow structure. The shell thickness and cavity can be easily identified. Compared with Figure 4d, Figure 4e clearly reveals an increase of gold shell thickness and a decrease in interior-cavity size. It is evident from Figure 4f that gold solid nanoparticles with an average diameter of 60.0 ± 6.1 nm were

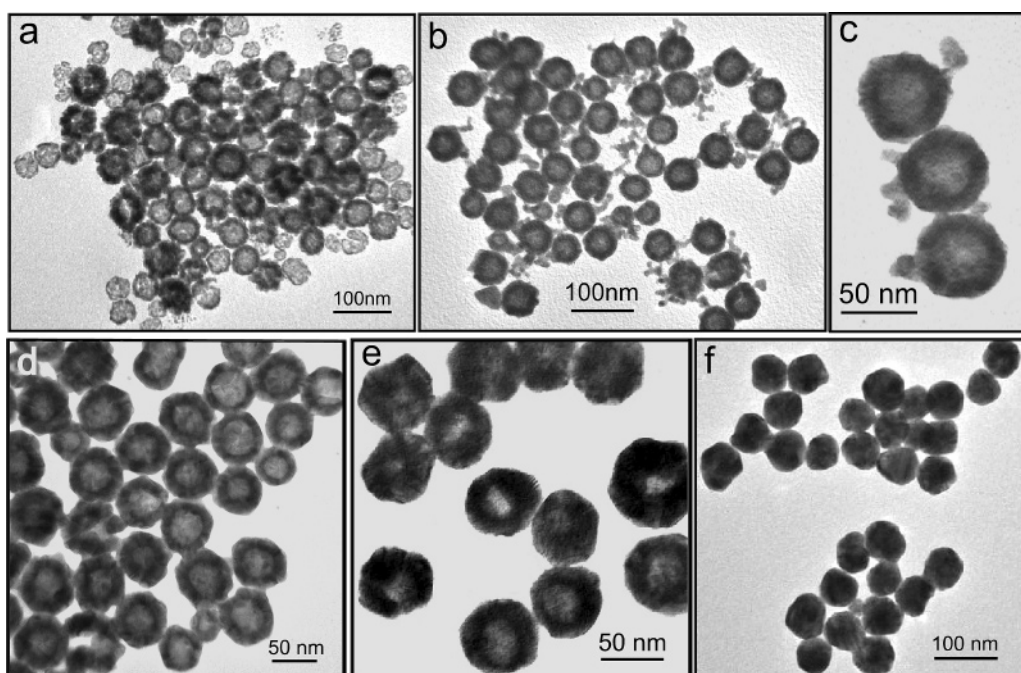


Figure 4. (a, b) Low-magnification TEM images of samples A and C, respectively. (c–f) High-magnification TEM images of samples C, B, D, and E, respectively.

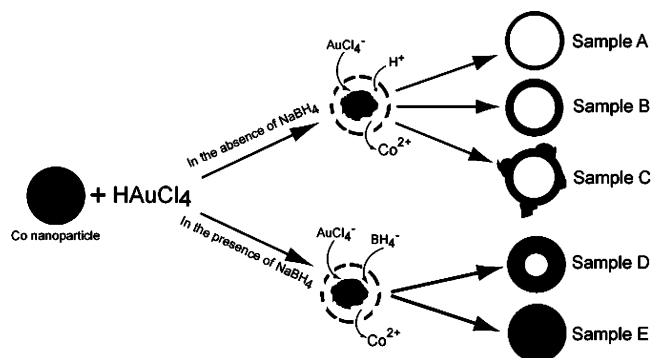
TABLE 1: The Average Outer and Inner Diameter, Shell Thickness, and Wavelength of SPR Peaks of the Various Gold Hollow and Solid Nanospheres (samples A–E)

	sample A	sample B	sample C	sample D	sample E
outer diameter (nm)	59.2 ± 7.8	58.6 ± 4.5	59.0 ± 5.2	58.8 ± 6.4	60.0 ± 6.1
inner diameter (nm)	40.0 ± 5.1	28.6 ± 3.0	29.0 ± 3.1	14.6 ± 2.6	0
shell thickness (nm)	9.6 ± 4.3	15.0 ± 2.0	15.0 ± 1.8	22.1 ± 3.0	30.0 ± 2.8
wavelength of SPR peaks (nm)	628	595	592	550	526

formed. Since the outer diameters are controlled by the diameter of Co nanoparticles, the outer diameters of these hollow nanospheres are largely identical. Table 1 summarizes the average outer and inner diameters, shell thickness, and wavelength of SPR peaks of these hollow and solid nanospheres. These results, together with the nanostructures in Figure 4a,d,e,f, clearly reveal an inward growth process of gold hollow nanospheres.

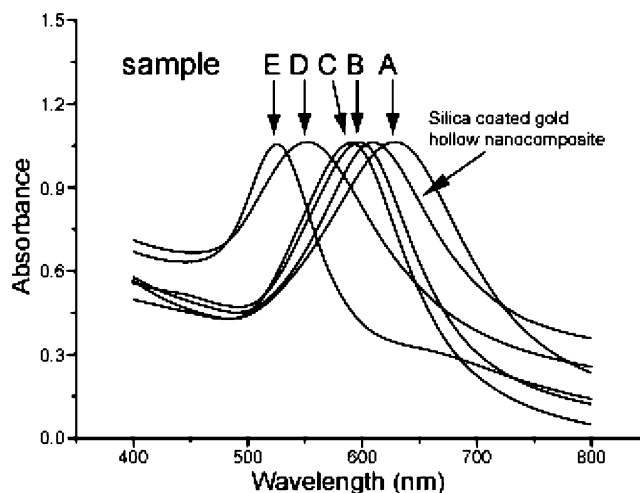
The changes in these nanostructures are also reflected in the coloration of these aqueous suspensions. The color of samples A, B, and C was blue, while the color of samples D and E was purplish red and pink, respectively. In general, gold hollow nanospheres with tunable interior-cavity size are achieved by changing the stoichiometric ratio of HAuCl_4 over the reducing agent(s). The process is clearly illustrated in Figure 5. In the absence of NaBH_4 in the Co colloidal solution, the main reactions are the reduction of Co nanoparticles by AuCl_4^- and H^+ . The shell formation is an inward growth process, in which the thickness of the gold shell increases inward as the replacement between Co nanoparticles and HAuCl_4 continues. The gold shell at its formation stage should have an incomplete porous structure because Co^{2+} and AuCl_4^- can continuously diffuse into the shell. The porous structure allows the remaining active Co “core” to be continuously oxidized to Co^{2+} by H^+ when there is not a sufficient supply of HAuCl_4 . In the presence of NaBH_4 in the Co colloidal solution, the process is mainly attributed to two distinct reduction reactions: namely, the initial reduction of HAuCl_4 by Co nanoparticles and the subsequent reduction of HAuCl_4 by NaBH_4 . The porous structure also enables BH_4^- diffusing into the cavity of hollow spheres to reduce AuCl_4^- to Au. Therefore, gold hollow shells here act as nanoreactors for the oxidation of Co nanoparticles and the reduction of AuCl_4^- . As a result, the shell grows inward until all of the HAuCl_4 was consumed, if the BH_4^- was in excess. These hollow spheres can eventually become solid ones if the appropriate volume of HAuCl_4 is used, as shown in Figure 4f. In such a circumstance, the solid nanoparticles grow outward as the common seed-mediated growth process if excess HAuCl_4 still remained.

Optical Characterization. The SPR properties of gold nanostructures are discernible in the UV–visible region. Figure 6 shows the UV–visible absorption spectra of aqueous solution

**Figure 5.** Schematic illustration of the formation process of Au hollow nanospheres with tunable interior-cavity size.

of samples A, B, C, D, and E with an increase of gold shell thickness. The characteristic SPR peaks show an evident blue shift from sample A to sample E due to the increase of gold shell thickness. The results are also summarized in Table 1. The SPR band of these hollow nanospheres can be tuned to cover the spectral region from 526 to 628 nm. The SPR peak at ca. 526 nm for sample E is similar to that of gold solid colloids with a diameter of 50 nm (SPR peak at ca. 528 nm).^{1c,19} The result further confirms that the gold nanostructure in sample E is a solid nanosphere rather than a hollow one. Consequently, the shift of SPR peaks can be attributed to changes in shell thickness. Since the shell thickness of these gold nanospheres are thinner than the mean free path (50 nm) of electrons in bulk gold, even a slight change in the shell thickness would significantly shift the wavelength of their SPR peaks.³ The results indicate that we have accomplished tunable SPR by controlling the interior-cavity size of gold hollow nanostructures.

Silica-Coated Gold Hollow Nanocomposites. Surface modification is a major challenge in metal nanoparticle preparation. The addition of an extra functionality onto each individual particle directly leads to a multifunctional nanoparticle and offers the opportunity to study the mutual interactions between the new functionality and the core materials. The surface modification of gold nanostructures to form silica coating is attractive because it opens up a wide range of surface modification chemistry that is not available for bare gold.²⁰ In the present study, silica-coated gold hollow nanocomposites are fabricated. Figure 7a is a low-magnification TEM image of silica-coated gold hollow nanocomposites. It can be seen that almost every single gold hollow nanosphere is completely coated with silica shell, which can be identified by contrast difference of these nanocomposites. The silica shell has a thickness of ca. 15 nm based on high-magnification TEM image (Figure 7b). These nanostructures remain as well-dispersed suspensions during the entire process of silica coating. As shown in Figure 7c, the energy-dispersive X-ray analysis (EDAX) of silica-coated gold hollow nanocomposites reveals the presence of silica, confirming the coating of silica. From the low- and high-magnification SEM

**Figure 6.** UV–visible absorption spectra of a suspension solution of samples A–E and silica coated gold hollow nanocomposites.

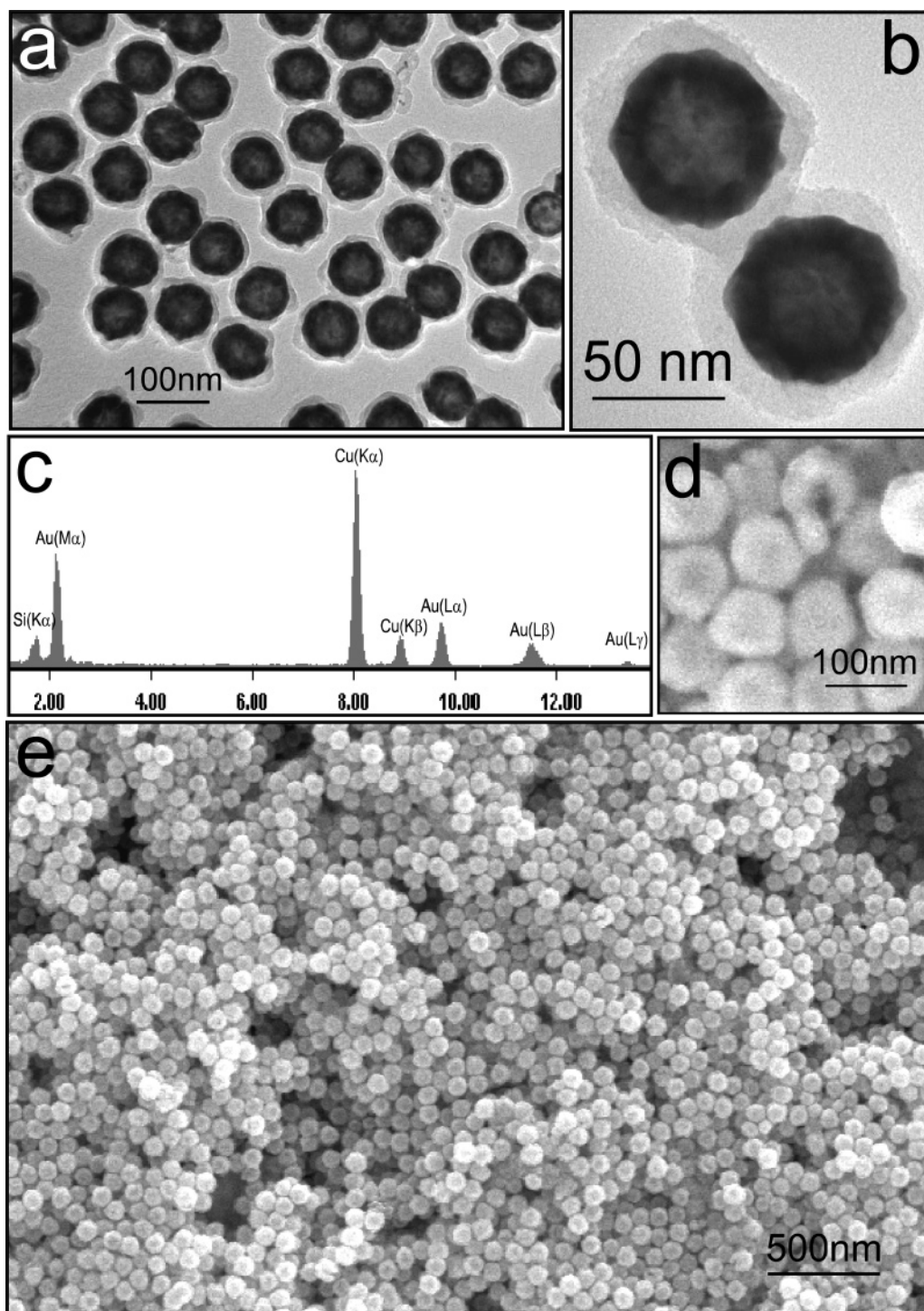


Figure 7. (a, b) Typical TEM and (d, e) SEM images of silica-coated gold hollow spheres. (c) The EDAX results of silica-coated gold hollow spheres.

images of the nanocomposites (Figure 7d,e), large-scale uniform spherical silica-coated gold hollow nanocomposites with an average diameter of 90 nm are fabricated. The UV–visible absorption spectrum of silica-coated gold hollow nanocomposites is shown in Figure 6, indicating that SPR peaks are red shifted compared with sample B.

Conclusion

In summary, we have demonstrated a facile and effective approach to fabricate gold hollow nanospheres with a tunable interior-cavity size using Co nanoparticles as sacrificial templates. The interior-cavity size can be controlled by varying the

stoichiometric ratio of HAuCl_4 over reducing agent(s). The gold hollow spheres act as nanoreactors for the oxidation of Co nanoparticles and the reduction of AuCl_4^- . The SPR peaks wavelengths corresponding to these hollow nanospheres are shifted and covered the spectral region from 526 to 628 nm. Silica-coated gold hollow nanospheres are also successfully fabricated, showing different SPR features.

Nanostructures with hollow interiors offer several advantages over their solid counterparts: namely, lightweight, reduction in material, and cost. In addition, the cavity provides a unique space as either reactor or store. Most previous synthetic methods of gold hollow nanostructures have resulted in low yields of

rough surfaced, polycrystalline products, which are considerably heterogeneous in shell thickness and composition. Our process affords a large-scale synthesis of well-defined, tunable void sizes that are homogeneous, smooth, and highly crystalline-walled nanostructures. These optically active plasmonic nanostructures are of great interest in basic research and in such diverse applications as photonic devices, drug delivery, microfluidic valves or pumps, and biology.

Acknowledgment. Financial support from National Natural Science Foundation of China (Nos. 20025308, 20177025, 10028408, and 20121301), National Key Project on Basic Research (Grant G2000077501), and the Chinese Academy of Sciences is gratefully acknowledged.

References and Notes

- (1) (a) Murphy, C. J.; Jana, N. R. *Adv. Mater.* **2002**, *14*, 80. (b) Kim, F.; Song, J. H.; Yang, P. *J. Am. Chem. Soc.* **2002**, *124*, 14316. (c) Link, S.; Mohamed, M. B.; El-sayed, M. A. *J. Phys. Chem. B* **1999**, *103*, 3073. (d) Jana, N. R.; Gearheart, L.; Murphy, C. J. *J. Phys. Chem. B* **2001**, *105*, 4065. (e) Daniel, M. C.; Astruc, D. *Chem. Rev.* **2004**, *104*, 293. (f) Grant, C. D.; Schwartzberg, A. M.; Norman, T. J., Jr.; Zhang, J. Z. *J. Am. Chem. Soc.* **2003**, *125*, 549.
- (2) (a) Liang, Z.; Susa, A.; Caruso, F. *Chem. Mater.* **2003**, *15*, 3176. (b) Carotenuto, G. *Appl. Organomet. Chem.* **2001**, *15*, 344. (c) Storhoff, J. J.; Elghanian, R.; Mucic, R. C.; Mirkin, C. A.; Letsinger, R. L. *J. Am. Chem. Soc.* **1998**, *120*, 1959. (d) Knoll, B.; Keilmann, F. *Nature* **1999**, *399*, 134. (e) Emory, S. R.; Nie, S. *Anal. Chem.* **1997**, *69*, 2631. (f) Brolo, A. G.; Gordon, R.; Leathem, B.; Kavanagh, K. L. *Langmuir* **2004**, *20*, 4813. (g) Schwartzberg, A. M.; Grant, C. D.; Wolcott, A.; Talley, C.; Huser, T.; Bogomolni, R.; Zhang, J. Z. *J. Phys. Chem. B* **2004**, *108*, 19191.
- (3) Sun, Y.; Xia, Y. *Anal. Chem.* **2002**, *74*, 5297.
- (4) (a) Prodan, E.; Radloff, C.; Halas, N. J.; Nordlander, P. *Science* **2003**, *302*, 419. (b) Hirsch, L. R.; Jackson, J. B.; Lee, A.; Halas, N. J.; West, J. L. *Anal. Chem.* **2003**, *75*, 2377.
- (5) Aden, A. L.; Kerker, M. *J. Appl. Phys.* **1951**, *22*, 1242.
- (6) (a) Caruso, F.; Caruso, R. A.; Möhwald, H. *Science* **1998**, *282*, 1111. (b) Jiang, P.; Bertone, J. F.; Colvin, V. L. *Science* **2001**, *291*, 453.
- (7) (a) Kim, S.-W.; Kim, M.; Lee, W. Y.; Hyeon, T. *J. Am. Chem. Soc.* **2002**, *124*, 7642. (b) Dai, Z.; Dähne, L.; Möhwald, H.; Tiersch, B. *Angew. Chem., Int. Ed.* **2002**, *41*, 4019.
- (8) (a) Bourlino, A. B.; Karakassides, M. A.; Petridis, D. *Chem. Commun.* **2001**, 1518. (b) Schmidt, H. T.; Ostafin, A. E. *Adv. Mater.* **2002**, *14*, 532.
- (9) (a) Nakashima, T.; Kimizuka, N. *J. Am. Chem. Soc.* **2003**, *125*, 6386. (b) Fowler, C. E.; Khushalani, D.; Mann, S. *Chem. Commun.* **2001**, 2028. (c) Gao, X.; Zhang, J.; Zhang, L. *Adv. Mater.* **2002**, *14*, 290.
- (10) (a) Schacht, S.; Huo, Q.; Voigt-Martin, I. G.; Stucky, G. D.; Schuth, F. *Science* **1996**, *273*, 768. (b) Sun, Q.; Kooyman, P. J.; Grossmann, J. G.; Bomans, P. H. H.; Frederik, P. M.; Magusin, P. C. M. M.; Beelen, T. P. M.; van Santen, R. A.; Sommerdijk, N. A. J. M. *Adv. Mater.* **2003**, *15*, 1097. (c) Jang, J.; Lee, K. *Chem. Commun.* **2002**, 1098. (d) Zhang, D.; Qi, L.; Ma, J.; Cheng, H. *Adv. Mater.* **2002**, *14*, 1499.
- (11) (a) Sun, Y.; Xia, Y. *Science* **2002**, *298*, 2176. (b) Sun, Y.; Mayers, B. T.; Xia, Y. *Adv. Mater.* **2003**, *15*, 641. (c) Sun, Y.; Mayers, B. T.; Xia, Y. *Nano Lett.* **2002**, *2*, 481.
- (12) Yang, Z.; Niu, Z.; Lu, Y.; Hu, Z.; Han, C. C. *Angew. Chem., Int. Ed.* **2003**, *42*, 1943.
- (13) Liang, H.-P.; Zhang, H.-M.; Hu, J.-S.; Guo, Y.-G.; Wan, L.-J.; Bai, C.-L. *Angew. Chem., Int. Ed.* **2004**, *43*, 1540.
- (14) Kobayashi, Y.; Horie, M.; Konno, M.; Rodríguez-González, B.; Liz-Marzán, L. M. *J. Phys. Chem. B* **2003**, *107*, 7420.
- (15) Stöber, W.; Fink, A.; Bohn, E. *J. Colloid Interface Sci.* **1968**, *26*, 62.
- (16) Lisiecki, I.; Pileni, M. P. *Langmuir* **2003**, *19*, 9486.
- (17) Glavee, G. N.; Klabunde, K. J.; Sorensen, C. M.; Hadjipanayis, G. C. *Langmuir* **1993**, *9*, 162.
- (18) Frens, G. *Nature* **1973**, *241*, 20.
- (19) Lu, Y.; Yin, Y.; Li, Z.-Y.; Xia, Y. *Nano Lett.* **2002**, *2*, 785.
- (20) (a) Dick, K.; Dhanasekaran, T.; Zhang, Z.; Meisel, D. *J. Am. Chem. Soc.* **2002**, *124*, 2312. (b) Nooney, R. I.; Thirunavukkarasu, D.; Chen, Y.; Josephs, R.; Ostafin, A. E. *Langmuir* **2003**, *19*, 7628.